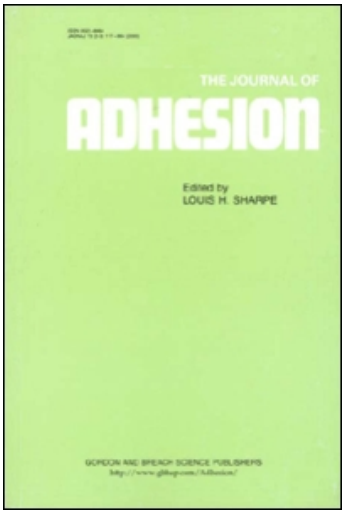

The Journal of Adhesion
Publication details, including instructions for authors and subscription information:
http://www.informaworld.com/smpp/title~content=t713453635

On the Nature of the Multi-Zone Interphase of a Thermoset/Thermoplastic Composite-An Analysis Employing Dynamic-Mechanical Thermal Analysis and Nanoindentation

M. Munz[a]
[a] National Physical Laboratory (NPL), Quality of Life Division, Teddington, Middlesex, UK

To cite this Article Munz, M.(2008) 'On the Nature of the Multi-Zone Interphase of a Thermoset/Thermoplastic Composite-An Analysis Employing Dynamic-Mechanical Thermal Analysis and Nanoindentation', The Journal of Adhesion, 84: 5, 445 — 482
To link to this Article: DOI: 10.1080/00218460802089312
URL: http://dx.doi.org/10.1080/00218460802089312

The Journal of Adhesion, 84:445–482, 2008
ISSN: 0021-8464 print/1545-5823 online
DOI: 10.1080/00218460802089312

Taylor & Francis
Taylor & Francis Group

On the Nature of the Multi-Zone Interphase of a Thermoset/Thermoplastic Composite–An Analysis Employing Dynamic-Mechanical Thermal Analysis and Nanoindentation

M. Munz
National Physical Laboratory (NPL), Quality of Life Division, Teddington, Middlesex, UK

As a model system for a thermoplastic/thermosetting composite material, a stoichiometric amine-epoxy formulation was cured in the presence of the thermoplastic poly(vinylpyrrolidone) (PVP). The epoxy system consisted of the resin diglycidyl ether of bisphenol A (DGEBA) and the aromatic curing agent 4,4′-diaminodiphenylsulfone (DDS). Using nanoindentation, profiles of the sample Young's modulus, E_s, the hardness, H, as well as the plasticity index, ψ, were measured and found to show significant variations. From the hardness profile three different interphase (IP) zones can be identified. They add up to a total interphase width of $\sim$230 microns. Further information on the nature of the interphasial zones was deduced from temperature-dependent dynamic mechanical thermal analysis (DMTA) and energy-dispersive analysis of X-rays (EDX). In particular, the outer edge of zone Z2 is consistent with the width of the amine depletion zone. Finally, the different IP zones are discussed in terms of the diffusion processes taking place during the epoxy curing procedure.

Keywords: Adhesion; Creep; DMA/DMTA; EDX/EDS; Epoxy; Hardness; Interdiffusion; Interphase/Interface; Nanoindentation; Plasticity; Polymer; Thermoplastic; Thermosets; Viscoelasticity; Young's modulus

Received 5 November 2007; In final form 27 March 2008.

Presented in part at the 3rd World Congress on Adhesion and Related Phenomena (WCARP-III), Beijing, PR China, 15–18 October, 2006.

Address correspondence to Martin Munz, National Physical Laboratory (NPL), Quality of Life Division, Hampton Road, Teddington, Middlesex TW11 0LW, UK. E-mail: martin.munz@npl.co.uk

INTRODUCTION

A major contribution to the adhesion between two thermoplastics is the diffusion of chain elements across their mutual interface. Apart from enthalpic driving forces, such as acid-base interactions depending on the particulars of the polymers involved, entropic penalties arising from restrictions of chain configurations in a steep concentration gradient drive the transfer of chains across the interface [1]. Such mutual interdiffusion or other interfacial interactions result in the formation of an interphase (IP), *i.e.*, a three-dimensional region of variations in structure and properties and of major relevance for the strength of the bond between the two polymer parts [2]. The annealing conditions are crucial for the extent of diffusion-enhanced bonding. As pointed out by Schreiber and Ouhlal [3], the high throughput rates typical for mass production often allow for only short annealing periods at the favourable temperatures and pressures. As a consequence, frequently the requirements for effective interdiffusion are not met under such conditions, and this may lead to the erroneous perception of diffusion being of minor importance for development of adhesion strength.

In the case of thermosetting systems, such as amine-cured epoxy, the formation of an IP is affected by the thermodynamic driving forces favouring enrichment of a certain component as well as by the kinetics of the curing reaction. If prepared from a low-viscosity mixture of the prepolymer and a curing agent, the high mobility of the comparatively small molecules results in large diffusion lengths. For instance, in their study of the diffusion of amine and epoxy in polysulfone, Immordino *et al.* [4] reported diffusivity values in the range of 10^{-9}–10^{-12} cm^2/s, *i.e.*, one to two orders in magnitude larger than for the reptation of high polymers. In particular, the diffusivity of amine was found to be an order of magnitude larger than for epoxy [4].

It is worthwhile mentioning that apart from the interdiffusion across an initially sharp interface between a thermoplastic and a curing thermosetting system, provided a sufficient molecular mobility, also demixing of a homogeneous blend can occur and lead to two-phase morphologies [5–7]. This is the case when a driving force for phase separation builds up in the course of the curing process. In many cases the miscibility decreases with increasing crosslink density, and such a reaction-induced phase separation can be exploited to tailor the mechanical properties of the cured system as well as to create complex morphologies [5–7]. Rheological measurements performed upon curing were found to reveal the segregation processes through significant changes in the viscoelastic properties [8,9].

As a result of the ongoing crosslinking reaction, the average molecular weight increases, leading to a rise in the viscosity and a decrease in the molecular mobility. As demonstrated by Palmese and McCullough [10] as well as by Yang and Pitchumani [11], for thermosetting systems the final width of the interphasial concentration variations can be strongly affected by the so-called Damköhler number, *i.e.*, the ratio of the curing rate and the diffusion rate. This appears to be one of the major reasons for the strong variation in epoxy IP widths reported in the literature, ranging from several hundreds of nanometres to several tens of microns [12–15].

Furthermore, the final concentration profile is not necessarily monotonic. For instance, in the case of a preferential adsorption of the curing agent at the interface with the substrate, the thermodynamic driving forces result in a locally increased amine concentration. Due to the conservation of mass, however, the additional amine molecules need to be provided from the bulk, *i.e.*, from the amine-epoxy mixture farther away from the interface. The enrichment of amine molecules at the interface can lead to an adjacent depletion zone that needs to be refilled from the bulk [11]. Given sufficient time for the required mass transport, the refilling occurs to full degree and a monotonic concentration profile will be observed, as measured in the direction perpendicular to the interface. This is the case for a slow curing reaction as compared with the diffusion of molecules. In the opposite case, however, the rapid rise in viscosity slows the diffusion downand, in part, the depletion zone will be conserved. As a consequence, the final concentration profile will be non-monotonic, including a zone of high amine concentration adjacent to the interface and a zone depleted in amine, located between the enrichment zone and the bulk epoxy. Essentially, it can be concluded that the kinetics of the processes involved affect both the IP width and the form of the IP concentration profile. In the past, techniques of chemical mapping or profiling were employed for studying such effects, for instance by means of infrared spectroscopy [14,16,17] or energy-dispersive analysis of X-rays (EDX) [12,18,19].

Although such concentration profiles may provide valuable insight into interfacial phenomena, additional knowledge of the local variations in physical properties such as stiffness or frictional behaviour can be of particular interest. The aim of the present study was to provide a detailed characterisation of the variations in the mechanical properties of an epoxy IP, using a nanoindentation set-up equipped with a Berkovich tip (indenter). In addition, a comparatively wide IP was generated, thus avoiding any complications resulting from the finite size of the indenter. Due to the lateral extent of the stress

distribution beneath the indenter, an indentation experiment performed in the vicinity of an interface can be affected by the adjacent phase [20,21]. Such a mechanical bias effect occurs within a zone of finite width. Care has to be taken not to confuse interphasial property variations with variations related to the mechanical bias effect. In particular, this impediment matters if the width of the IP is smaller than, or comparable with, the width of the zone of the mechanical bias effect [22].

The results from the nanoindentation measurements are corroborated by data elucidating the existence and the effect of variations in the amine-epoxy concentration ratio. Local variations in the amine concentration were measured using EDX, and the dependence of the epoxy elastic properties on the amine-epoxy concentration ratio was studied using dynamic-mechanical thermal analysis (DMTA).

In particular, the system under investigation was a thermoplastic/thermosetting system consisting of the thermoplastic poly(vinylpyrrolidone) (PVP) and the epoxy diglycidyl ether of bisphenol A (DGEBA) cured with diaminodiphenylsulfone (DDS). PVP is an amorphous vinyl polymer with a pendant lactam ring. The latter contains a carbonyl group, which renders PVP likely to interact with the amine-epoxy system *via* hydrogen bonds [12]. In the vicinity of an interface, this interaction is likely to act as a driving force for diffusion processes.

In their seminal study of this epoxy/thermoplastic system, Oyama *et al*. observed IP concentration variations of the amine curing agent, indicating partial absorption of the amine by the PVP layer *via* interdiffusion processes. These take place during the curing of the epoxy in the presence of the thermoplastic [12]. By mixing the standard DGEBA with brominated DGEBA, in EDX the Br-signal allowed spatial epoxy concentration variations to be tracked. From the combined analysis of the N-, S-, and Br-signals, concentration profiles for PVP, DDS, as well as DGEBA were deduced. The width of the concentration profiles was shown to increase with the temperature of the initial cure stage (130 and 170°C) as well as with decreasing molecular weight of PVP. The initial stage of the two-step curing cycle (post-curing at 220°C) was decisive for the interdiffusion processes [12,18]. Furthermore, from their analysis of the concentration profiles of each species Oyama *et al.* [12] concluded that the diffusion front of DDS was located several microns farther into the PVP layer than that of epoxy.

In a wider sense, the system under investigation can be considered as a model for a thermoplastic part coated with a two-component thermoset or for a thermosetting adhesive connecting thermoplastic adherends. Applications of thermoplastics as sizing materials for fibres embedded in a thermosetting matrix were demonstrated also [23].

EXPERIMENTAL

Polyvinylpyrrolidone (PVP) films were prepared using powder of PVP as supplied by Fluka (Buchs, Switzerland). For the chemical structure of PVP see Fig. 1. The K-90 grade corresponds to a number average molecular weight $M_n \sim 360000$ (viscosity average molecular weight $M_v = 1100000$) [24]. PVP was dissolved in a 1:1 mixture by volume of distilled water (grade pro analysi, by Merck, Darmstadt, Germany) and methanol (grade pro analysi, by Riedel-de-Haen, Seelze, Germany). About 5.5 g of PVP were dissolved in 40 mL of the water-methanol mixture. From this solution, films were cast into Teflon® moulds. For the purpose of drying, these films were stored for two weeks at RT and for another two weeks at 80°C. In order to avoid stress-induced cracking of the films, the process of drying was slowed down by keeping the gas exchange to a minimum. The moulds were stored in covered beakers with only small openings. Differential scanning calorimetry (DSC) measurements of such PVP films delivered a glass transition temperature, T_α, of $\sim(172 \pm 4)$°C, as taken at the centre of the transition. The heating rate of the DSC measurements was 10°C/min. From the onset glass transition temperature of ~ 158°C of the PVP films (as measured using DSC) and from the data published by Tan and Challa [25], it can be concluded that the water content of these PVP films was ~ 1.7 wt% before the final drying step at ~ 110°C was undertaken. Considering the data given [25], a decrease in T_α of ~ 9.8°C per wt% of water can be deduced, and the

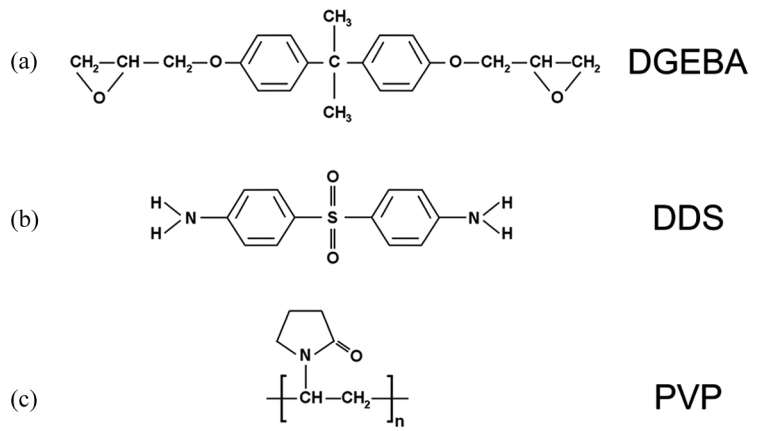

FIGURE 1 Molecular structure formulae of (a) the epoxy resin DGEBA, (b) the curing agent DDS, and (c) the thermoplastic PVP, respectively.

extrapolated value of the onset T_α for a water content of zero is $\sim$175°C.

The final thickness of the PVP films was in the range of 50–150 μm, as measured by means of scanning electron microscopy (SEM) images as well as by atomic force microscopy (AFM) topography (see Fig. 10a) images of cross-sections of the sandwich-like samples.

The epoxy resin used (Fig. 1) was of type diglycidyl ether of bisphenol A (DGEBA) with a condensation factor, n, of the higher molecular weight homolog close to zero, namely DER332 (Dow Chemical, Stade, Germany). According to $n \sim 0$, the average epoxy equivalent weight (EEW) of DER332 (EEW $\sim$174 g/mol) is almost identical to that of chemically pure DGEBA (EEW $\sim$170 g/mol) [26]. The diamine curing agent used (Fig. 1) was 4,4′-diamino-diphenylsulphone (DDS; grade purum, $\geq$97.0% [NT], Sigma-Aldrich, Munich, Germany), the molecular weight of which is given by the manufacturer as 248.3 g/mol.

The DGEBA as well as the DDS molecule contains two units of the respective chemical groups responsible for the curing reaction, namely, the epoxy (oxirane) group and the primary amine group, respectively (see Fig. 1). These reactive groups are situated at the ends of the molecules. Since one primary amine group is expected to react with two epoxy (oxirane) groups, $N_e = 2$ mol of DGEBA correspond to $N_a = 1$ mol of DDS. Thus, the amine-epoxy mixing ratio, r, can be defined as follows [27]:

$$r = \frac{N_a}{N_e} \cdot \frac{f_a}{f_e}, \tag{1}$$

where f_a and f_e denote the chemical functionalities of the amine and the epoxy molecules, respectively. The corresponding values for DDS and DGEBA are $f_a = 4$ and $f_e = 2$. Essentially, two different concentration regimes are discernible, namely, the under-stoichiometric regime (where epoxy is in excess) and the over-stoichiometric regime (where amine is in excess). These regimes are given by $r < 1$ and $r > 1$, respectively. The demarcation $r = 1$ denotes the stoichiometric case (equimolar ratio). For the purpose of studying the relationship between stoichiometry and mechanical properties of the cured epoxy, samples of different concentration ratios were prepared, with r ranging from 0.6 to 2.0.

The isothermal curing temperature of 170°C was close to the glass transition temperature, T_α, of the PVP film. For the DGEBA-DDS system, the final degree of cure achievable at 170°C is $\sim$85% [27], which is reached after $\sim$120 min. After this period of time, the beaker containing the epoxy formulation was removed from the oil bath and

cooled down to RT. It should be noted that the ultimate glass transition temperature, $T_{\alpha\infty}$,, of the fully cured DGEBA-DDS system is $\sim$218°C [28]. Such a condition was achieved by post-curing at $\sim$220°C for 1 h (after it had been cured for 2 h at 170°C). For such a sample, DSC measurements delivered for T_α an onset value of $\sim$219°C and a peak value of $\sim$225°C. The heating rate of this measurement was 2°C/min. Thus, in order to circumvent vitrification and the resulting diffusion-control of the reaction rate, a curing temperature higher than 170°C is required for achieving $T_{\alpha\infty}$. However, no such post-curing step was applied to avoid oxidative effects taking place in PVP [19].

For purpose of curing of the epoxy system in the presence of the PVP film a stack of Teflon moulds was developed which fits into a 400 mL glass beaker. The lower half of the glass beaker was immersed into a temperature-controlled oil bath (type TP-6, Julabo Labortechnik, Seelbach, Germany). The loaded stack was inserted into the glass beaker after the homogenised mixture of epoxy resin and curing agent was prepared. While heating and stirring the ingredients, the glass beaker was capped by a lid, and a gentle flow of nitrogen was applied to protect the epoxy-amine mixture against oxidation. For stirring, a glass rod was fed through a sealed opening in the lid of the beaker. The time-temperature scheme for mixing and curing was as follows. Firstly, the liquid epoxy resin was added at 50°C, heated up to 110°C within 10 min, and kept at this temperature for 60 min to reduce the amount of water potentially absorbed in the course of the storage of the epoxy. Secondly, the appropriate amount of DDS powder was added at 110°C and the system was heated up to 160°C within 8 min. At this temperature, DDS dissolved very well in DER332 while the low-viscosity mixture was thoroughly stirred over 7 min. Then, the stack of Teflon moulds loaded with dried PVP films was inserted. Before, it was kept at a temperature of $\sim$110°C for 120 min while a gentle flow of nitrogen was applied. This allowed for a final drying of the PVP films. For purpose of isothermal curing of the epoxy, the loaded beaker was kept at a temperature of 170°C for 120 min. Afterwards, the beaker was removed from the oil bath to cool down to RT. Further details of the preparation procedure as well as of the EDX measurements are given in Reference [19].

A beam-shaped DMTA sample of dimensions $60 \times 10 \times 0.6\,\text{mm}^3$ was prepared by polishing an epoxy bar of initial thickness of $\sim$8 mm. The epoxy bar was fixed by a home-made sample holder with adjustable chucks. This sample holder was gently pressed against an emery paper (of grade 4000) on top of the turntable of a polishing machine (Struers, Copenhagen, Denmark). No flow of water was applied during

the polishing to protect the sample against the uptake of water. The emery paper was cleaned at regular time intervals. Care was taken to keep the thickness variations across the final DMTA beams as low as possible. Using such beams, DMTA measurements in torsional pendulum configuration (model ATM-3, Myrenne Instruments, Roetgen, Germany) were run in the temperature range from -180–$+270^{\circ}$C. For each beam, both a heating and a subsequent cooling scan were undertaken. The heating and cooling rates were $\sim \pm 1.1$ K/min, respectively. The frequency of the freely oscillating torsional pendulum was ~ 1 Hz.

Cross-sections of the epoxy-PVP-epoxy samples were prepared using an ultramicrotome (Ultracut UCT, Leica Mikrosysteme GmbH, Vienna, Austria). The microtoming was performed at RT, using a diamond knife of type Ultra30 (Diatome, Biel, Switzerland).

The nanoindentation experiments were performed using a commercial indenter setup (model Triboscope, Hysitron, Minneapolis, MN), combined with a home-built imaging system [29]. The measurements were made at room temperature, *i.e.*, around 22°C. The indenter was of the Berkovich type, *i.e.*, a three-sided pyramid with an ideal projected area-to-depth function given by the square of the depth of contact [22,30–32]. The opening angle from edge to face is $\theta = 65.3^{\circ}$ [31,32]. Due to blunting of the apex of the tip, however, deviations from the ideal area-to-depth function have to be taken into account. The particular area-to-depth function of the indenter was determined by means of a reference sample, which was an epoxy with a Young's modulus value of ~ 3.08 GPa (as resulting from a DMTA measurement of that reference material). For a given maximum load, the usage of a reference material of similar mechanical properties ensures a similar depth of indentation. In general, an extrapolation of tip shape data to larger depths can lead to uncertainties in the indentation measurements [32]. Such an extrapolation is required when applying the area-to-depth function derived from measurements on a stiff reference material to a compliant material.

The maximum load of the force-penetration curves was ~ 9.7 mN, resulting in a typical penetration depth of $\sim 1.4\,\mu$m. The rate of loading and unloading was 2 mN/s. For each indentation experiment, a hold period of 30 s was inserted between the loading and the unloading step, in order to allow for viscoelastic creep effects to occur before the unloading step was started. Otherwise, it could happen that a large amount of creep is superimposed on the elastic displacements recovered during unloading [33].

The indents were arranged along parallel lines oriented perpendicular to the interfacial borderline between the epoxy and the PVP. Within

the lines of indentations, the average and the lowest distance between neighbouring indents were 15.0 and 8.9 μm, respectively. The total extent of the field of indentations was $\sim 810 \times 170\,\mu m^2$. At each indentation point a force-penetration curve, $P(h)$, was recorded and evaluated.

The position of the demarcation line between IP and bulk epoxy was defined by a deviation of 1% from the bulk value of the epoxy Young's modulus (in the following referred to as 1% criterion). A lower value of the deviation limit seems not to be recommendable, since the determination of the IP width may be severely affected by the rate of convergence of the profile to the bulk value.

The calculation of smoothed interpolation splines (Figs. 3, 4, 5, 6b, 11, 12, 13b) was done using the Savitzky-Golay method as implemented in the software TableCurve2D (Systat Software Inc., Richmond, CA, USA).

The sample preparation, the measurements, as well as major parts of the data evaluation were performed at the Federal Institute for Materials Research and Testing (Bundesanstalt für Materialforschung und –Prüfung, BAM) in Berlin, Germany.

OFF-STOICHIOMETRY EFFECTS STUDIED BY MEANS OF DYNAMIC MECHANICAL THERMAL ANALYSIS (DMTA)

The viscoelastic properties of the epoxy are likely to change with the stoichiometric imbalance between epoxy resin and curing agent. In particular, knowledge of the relationship $E(r)$ is required in order to be able to convert the concentration profile into a modulus profile which then can be compared with the modulus profile measured using nanoindentation. Although this relationship $E(r)$ is required for the RT first of all, DMTA was performed in order to develop a deeper insight into the factors governing the viscoelastic properties of the epoxy.

A concentration series of epoxy samples was investigated employing DMTA. All the epoxy samples of the series were cured in the same manner (*i.e.*, for 2 h at 170°C), but differed in the amine-epoxy concentration ratio, r. The r values of these samples ranged from 0.6–2.0. The respective DMTA curves are given in Fig. 2. In each case, the temperature was scanned from -180–$+270$°C (heating scan, see Figs. 2a and 2b) and then scanned back (cooling scan, see Figs. 2c and 2d). The curves of the storage modulus, G', are displayed in the Figs. 2a and 2c and those of the loss modulus, G'', are displayed in the Figs. 2b and 2d.

Three distinct features can be readily observed from Fig. 2a:

(i) a significant spread in the glass transition temperatures, T_α, ranging from $\sim$75–200°C;

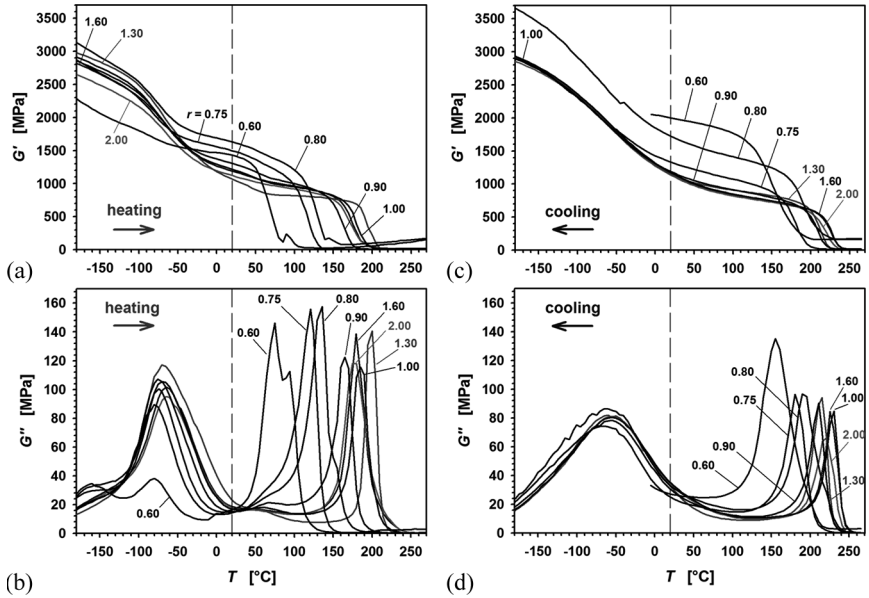

FIGURE 2 Dynamic-mechanical thermal analysis (DMTA) of the series of reference epoxy samples. The samples differ from each other in their amine-epoxy concentration ratios, r. The temperature range between -180 and $+270$°C was scanned in both directions. The curves resulting from the heating and the cooling scans are shown in (a), (b) and (c), (d), respectively. Figures (a) and (c) give the curves of the storage modulus, G', whereas (b) and (d) give the loss modulus, G''. For the purpose of easier consideration, the number of curves shown has been restricted by omitting the curves for the concentration ratios $r = 0.70$, 0.85, 1.10, 1.25, 1.40, and 1.80. The full set of curves is given in Ref. [14]. Strong variations in the α-transitions (around 170°C) can be observed between the samples of different r values. For the curves measured upon heating, also pronounced variations in the β-transitions (around -70°C) are observed. As visible from (a), the storage modulus at RT (20°C) is significantly increased for low values of r. When comparing the G' curves of three samples of the nominal amine-epoxy concentration ratio $r = 1$, the uncertainties in T and in G' are ~ 7°C and ~ 70 MPa, respectively. One of these curves is qualitatively similar to the curve for the $r = 1.1$ sample (glass transition at a higher temperature and a lower G' value at 20°C), and linear scaling of the shifts in T and G' delivers an error in r of $\sim 5\%$.

(ii) a pronounced variation in the storage modulus measured at RT, $G'(20°C)$ (as marked by a vertical dashed line at 20°C); and
(iii) a remarkable suppression of the β-transition (the centre of which is located between ~ -80 and ~ -60°C).

For each of the observations (i)–(iii), the variations are most pronounced for the samples with $r < 1$. Within this regime, reduction of r results in a decrease in T_α, an increase in $G'(20°C)$, and a decrease in the relaxation strength of the β-transition. In particular, the latter finding is obvious from the respective G'' curves (Fig. 2b), where the maximum value of the G''_β peak is strongly reduced for $r < 1$.

The changes in the glassy storage modulus, G', with departure from the stoichiometric ratio $r = 1$ are summarised in Fig. 3, where $G'(20°C)$ is plotted *versus* r. In the regime $r < 1$ a pronounced increase in $G'(20°C)$ is observed with decreasing values of r. In contrast, for the regime $r > 1$ no significant changes in $G'(20°C)$ can be stated.

For the purpose of comparison with the indentation experiments, the shear modulus was converted into Young's modulus, E, assuming isotropic behaviour and a Poisson's ratio, ν, of 0.42 [34]. The Young's modulus is given by $E = 2(1 + \nu)G$ [35]. In terms of the Young's modulus, for the data from heating scans the total change between $r = 1.0$

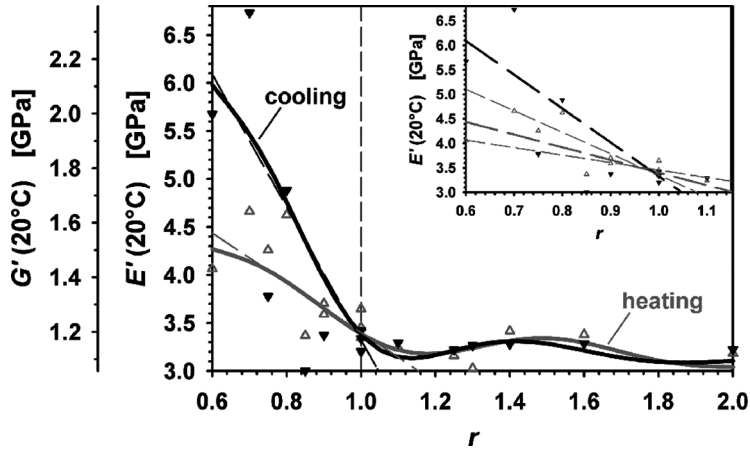

FIGURE 3 Modulus-concentration relationship, as extracted from Figure 2. The storage moduli G' and E' are plotted as a function of r, both for the heating (*grey*) and the cooling (*black*) scans. The E' values were calculated from the G' values assuming isotropic behaviour. The solid lines are splines to the measured data. In the range $r < 1$, the modulus values show a pronounced increase. The dashed lines represent linear approximations for the range $r < 1$. The minimum values occur slightly above the equimolar ratio, namely at $r \sim 1.2$ (heating) and $r \sim 1.1$ (cooling). For illustration of the uncertainties in the linear approximation for the regime $r < 1$ [Equations (2a) and (2b)], the inset shows the range of fits to the heating data; for comparison also the centre fit to the cooling data is shown.

and $r = 0.6$ is $\sim$1.0 GPa. Within the regime $r < 1$, the relationship $E'(r)$ can be approximated by linear equations:

$$E'_{heating} = (6.0 \pm 1.4) - (2.6 \pm 1.4) \cdot r \tag{2a}$$

$$E'_{\text{cooling}} = (10.2 \pm 5.1) - (6.9 \pm 5.0) \cdot r. \tag{2b}$$

The finding of increasing storage modulus with under-stoichiometric amount of amines may appear counter-intuitive, and it cannot be exclusively explained in terms of the crosslink density, since the $T_\alpha(r)$-curve reflects a decrease in the crosslink density with increasing stoichiometric imbalance (see *below*). However, apart from the crosslink density the elastic properties are also affected by the network topology and the corresponding packing density of elastically active bonds. In turn, the latter is presumed to show a strong influence on molecular dynamics. The corresponding relaxation behaviour is reflected by the DMTA measurements.

Similar observations were made by other authors studying off-stoichiometry effects in epoxies cured with aromatic amines. For the same system DER332/DDS, Meyer *et al*. [36] reported on a correlation where the minimum modulus value occurred at $r = 1$. In their case, the samples can be considered as fully cured since the curing schedule encompassed a post-curing step of 2 h at 220°C. Skourlis and McCullough found a similar relationship for DGEBA cured with PACM 20, a cyclo-aliphatic diamine with a molecular weight of 340 [37]. It should be noted that also in these studies the increase in the excess-epoxy side is more pronounced than on the excess-amine side. In a similar manner, Drzal *et al*. observed a minimum epoxy stiffness around the stoichiometric ratio of a DGEBA-type epoxy resin cured with meta-phenylenediamine (mPDA) [38].

For the glass transition temperature, T_α, and its changes with the concentration ratio, r, a bell-shaped curve is found, with the maximum occurring around the concentration ratio $r \sim 1.2$ (Fig. 4). According to Nielsen's approach [37,39], T_α can be described in terms of the average molecular weight between crosslinks, M_c:

$$T_\alpha - T_{\alpha u} = \frac{C}{M_c}, \tag{3}$$

where $T_{\alpha u}$ denotes the glass transition temperature of the uncured system and C is a constant factor. Neglecting side reactions, a maximum crosslink density, $1/M_c$, is presumed for fully cured stoichiometric systems, *i.e.*, in the case where all amine groups (primary as well as secondary ones) and epoxy groups are consumed by mutual

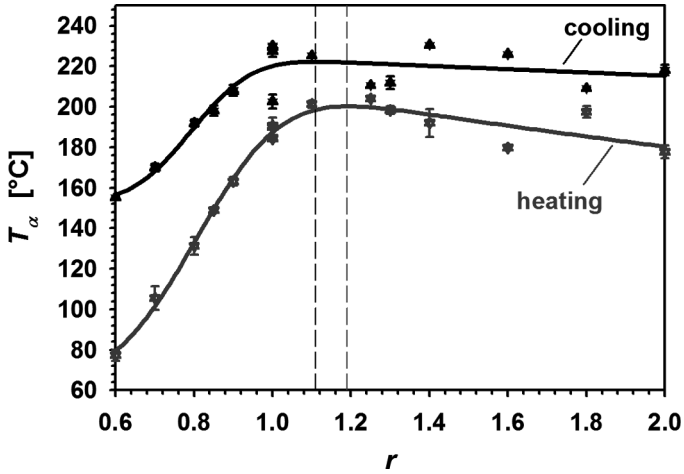

FIGURE 4 Variation of the glass transition temperature, T_α, with the concentration ratio, r. The curve is bell-shaped with the maximum around $r \sim 1.2$. The curve for the cooling scan is above the one for the heating scan, thus reflecting the increased crosslink density as a result of the post-curing taking place during the measurement. The T_α values were deduced from fits to the respective peak in G''. On average, the error in the readout of the peak position is less than ~ 2.6°C.

reactions. However, in cases of a stoichiometric imbalance either non-reacted epoxy groups (regime $r < 1$) or non-reacted amine groups (regime $r > 1$) remain, thus, resulting in a reduced average crosslink density. Due to their terminal position, non-reacted epoxy or primary amine groups represent dangling ends, each one of which comes along with an additional amount of free volume. Hence, the total free volume is increased and leads to a decrease in T_α with increasing deviation from the stoichiometric concentration ratio, $r = 1$ [36,37,40]. These plasticisation-like effects are the stronger the more reactive groups remain unconsumed.

In practice, the $T_\alpha(r)$ curve is frequently observed to be non-symmetric [40,41]. In the regime $r > 1$, there remain non-reacted primary or secondary amine groups. In general, primary amine groups exhibit a higher reaction rate than secondary amine groups [42]. If all the primary amine groups undergo reactions with epoxy groups, then no dangling ends of amine molecules will remain, even without any reaction of the secondary amine groups [41]. Additionally, as a result of their bulkier molecular structure, non-reacted epoxy groups are likely to make a larger contribution to the increase in the free

volume than incompletely reacted amine groups [40]. Thus, the case of excess amine is presumed to show less strong an effect on the resulting network structure than the opposite one of excess epoxy.

In a similar manner to T_α, the variation in the crosslink density can also be observed from the rubber modulus [39]. Indeed, a plot of the rubber storage modulus as measured at $T_\alpha + 60^\circ\text{C}$ delivered a curve similar to that of $T_\alpha(r)$ [19].

Another indication of dangling epoxy groups appears to be the emergence of a second loss peak (centred at $\sim -160^\circ\text{C}$) in the region of the β-transition. In particular, this observation is made for samples with $r < 0.8$ (Fig. 2b). Due to its almost separated appearance, in the following we refer to this peak as $\tilde{\beta}$-transition.

Indeed, the DMTA curves (Fig. 2) exhibit significant differences in the strength of the β-relaxation. Owing to the partial suppression of the β-transition for the samples with $r < 1$, the RT modulus of these samples is higher than that of the samples exhibiting a strong β-transition. Even though the storage modulus as measured below the β-transition is the lowest for the samples with $r < 1$, their respective RT modulus is the highest. This effect is reflected by the crossing of the $G'(T)$-curves in the high-temperature region of the β-transition.

The Role of the β-Transition

Considering the obvious importance of the β-transition, it is worthwhile taking a closer view. The changes in the centre temperature, T_β, as well as in the full width at half magnitude (FWHM), ΔT_β, of the β-transition are given in Fig. 5. With decreasing values of r (regime $r < 1$), the β-transition shifts to lower temperatures and its total width decreases. The DMTA curves (Fig. 2) reveal that it is mainly the high-temperature part of the β-transition which is suppressed. This effect can also be readily observed from a plot of the area of the G_β'' peak [19]. For the data measured upon heating, the curve is bell-shaped with the maximum located at $r \sim 1.3$. Thus, it is similar to the corresponding curves of T_α and $G_r'(T_\alpha + 60^\circ\text{C})$ [19]. Also, from this similarity, a dependence on the crosslink density can be inferred.

The difference between the total area of the G_β'' peak and the fit curves to the main G_β'' peak (which is centred at $\sim -70^\circ\text{C}$) increases with increasing departure from the concentration ratio $r \sim 1.2$ (Fig. 6). In Fig. 6a, the temperature range of the β-transition is shown for the case of a sample of concentration ratio $r = 0.75$. On the low temperature side of the G_β'' curve measured upon heating, a shoulder can be clearly seen. The area between this shoulder and a symmetric fit to the peak in G_β'' was calculated and plotted as a function of r

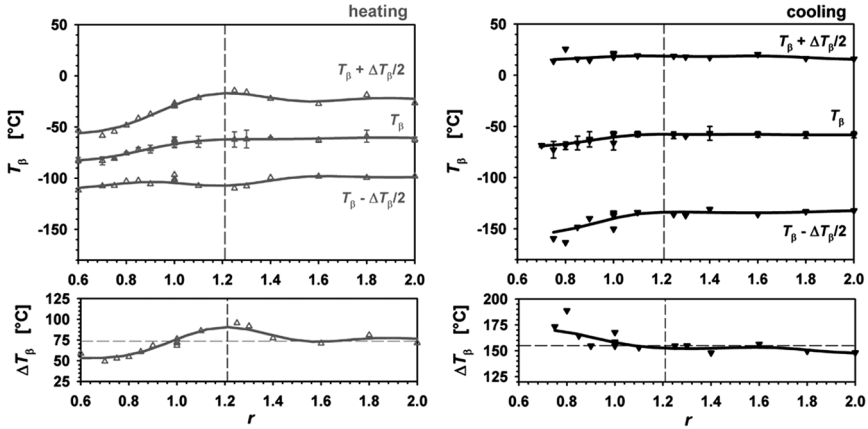

FIGURE 5 Variation in the β-transition with the concentration ratio, r. In the upper graphs, the characteristic temperatures $T_\beta - \Delta T_\beta/2$, T_β, and $T_\beta + \Delta T_\beta/2$ are shown. In the lower graphs, the respective FWHM values, ΔT_β, are displayed. The changes are given for both the heating (a) and the cooling (b) scans, respectively. For the heating scan, the largest FWHM is observed for r $\sim$1.2. For $r < 1$, T_β as well as ΔT_β decrease with increasing offset from the stoichiometric ratio $r = 1$, *i.e.*, a suppression of the β-transition is observed. The T_β values were deduced from fits to the respective peak in G''. On average, the error in the readout of the peak position is less than $\sim$4.1°C.

(Fig. 6b). The resulting curve shows a minimum around $r \sim 1.2$. In terms of the network structure, this finding reflects the existence of dangling ends and their particular dynamics, which becomes more relevant the larger the degree of off-stoichiometry. Notably, a significant contribution from dangling end motions occurs for the regimes of excess-epoxy as well as of excess-amine, although in the latter regime the effect is less pronounced. Together with the asymmetry of the $T_\alpha(r)$ curve (Fig. 4), it indicates that non-reacted ends of the DGEBA molecules show a much stronger effect on the elastic network properties than non-reacted or only partially reacted ends of the DDS molecules.

Presumably, the molecular dynamics of dangling epoxy groups is rather local and easier to be activated than such segmental motions which are severely restricted by the network of crosslinks. Indeed, the β-transition is frequently assigned to motions of the hydroxypropyl-ether sequence (-CH_2-CHOH-CH_2-O-), see [43] and the references given therein. These sequences result from the addition reaction of epoxy groups with amines, and their dynamics should be more restricted than that of dangling epoxy groups.

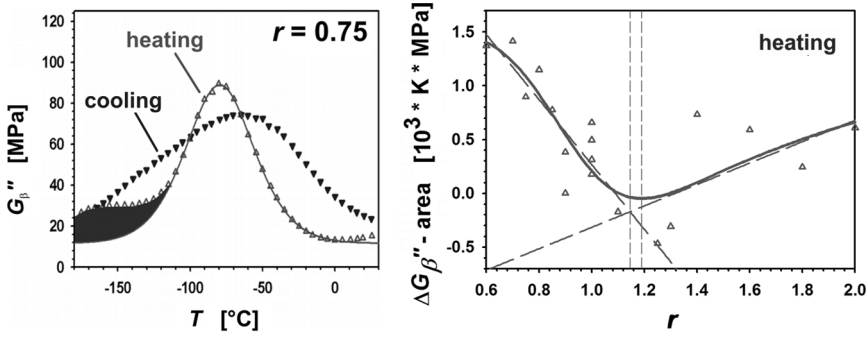

(a) (b)

FIGURE 6 Variation in the strength of the $\tilde{\beta}$ transition with the concentration ratio, r. (a) G_β" profiles for the case $r = 0.75$. The data measured upon heating and cooling are shown as light grey triangles (open) and as dark grey triangles (filled), respectively. The difference area between the measured curve and the fit to the main peak is filled with grey colour. (b) Plot of the difference area *versus* the concentration ratio. Linear fits to the data for $r \leq 1.1$ and $r \geq 1.1$ are in good agreement with the two branches of the smoothed curve. The intersection of the two lines is located at $r \sim 1.15$, and the minimum of the smoothed curve is located at $r \sim 1.19$.

As discussed by Heux *et al*. [44], the high-temperature part of the β-transition is related to local-scale cooperative motions. Consequently, the proportion of such cooperative motions can be presumed to decrease if the connectivity of the network is reduced, *i.e.*, if the constraints imposed by the network structure are partially released. In turn, the connectivity is linked to the crosslink density. Since the dense covalent network of a heavily crosslinked epoxy constitutes a highly coupled system, it needs high temperatures to entirely activate the relaxation mechanism [45]. In that sense, the observed suppression of the high-temperature part of the β-transition can be considered to be a result of the reduced crosslink density. Consistent with the above reasoning, from their calorimetric study of the α-transition Calventus *et al*. [40] deduced that the lower limit for the size of the cooperatively rearranging regions is greater for the stoichiometric system. In other words, off-stoichiometry implies that a smaller number of chain segments are involved in the relaxation process.

It should be noted that upon cooling the changes in the β-transition with the concentration ratio, r, follow a pattern that is different from the one observed upon heating. Upon cooling, the width of the β-transition is much larger, however, it exhibits comparatively little

changes with r (Fig. 5b). This finding is reflected by the total area of the G_{β}'' peak [19]. Also, there are no indications for a $\tilde{\beta}$-transition (Fig. 2d). Thus, within the regime $r < 1$ strong variations in the storage modulus values at RT, $G'(20^{\circ}C)$, occur but only moderate changes in the β-transition occur. In particular, within the regime $r < 1$ the $G'(20^{\circ}C)$ values measured upon cooling are higher than those measured upon heating. Such a deviation from the pattern attributed to antiplasticisation may be caused by a network topology differing from the one governing the behaviour upon heating. The strong increase in $G'(20^{\circ}C)$ with decreasing values of r (regime $r < 1$) indicates a large density of elastically loadable bonds. In addition to the chemical crosslinks, entanglements trapped by a high degree of topological constraints may contribute to the elastic modulus. Also, side-reactions may increase the number of crosslinks.

DETECTING GRADIENTS IN THE AMINE CONCENTRATION BY MEANS OF EDX

Starting from a stoichiometric and low-viscosity mixture of epoxy resin (DGEBA) and curing agent (DDS), the epoxy system was cured in the presence of the PVP film. The temperature of isothermal curing was 170°C. Driven by the preferential interaction of either DGEBA or DDS with PVP, spatial variations in the concentration ratio, r, can occur. Since the viscosity of the epoxy-amine mixture is rising fast with the degree of reaction, these effects are most likely to happen in the early phase of the curing procedure. From the point in time when gelation is reached and the viscosity diverges, however, any hitherto developed concentration gradients can be considered as frozen.

After the curing, cross-sectional surfaces of the epoxy/PVP/epoxy sandwich samples were prepared and investigated employing EDX. The orientation of the cross-sections was perpendicular to the epoxy/PVP interfaces. The Kα transition of the S contained in DDS provides a sufficient signal-to-noise ratio and can be used for tracking spatial variations in the DDS concentration. For the purpose of determining the particular concentration profiles, EDX measurements in line mode were run. The signals were recorded along lines perpendicular to the interfacial borderlines.

An example is shown in Fig. 7. By normalising the S- as well as the N-signal with the signal from the Ti Kα peak (Ti film thickness $\sim$36 nm), distortions of the profiles by potential temporal variations in the electron beam current were avoided. Such variations cannot be fully ruled out due to the long signal accumulation times of several hours.

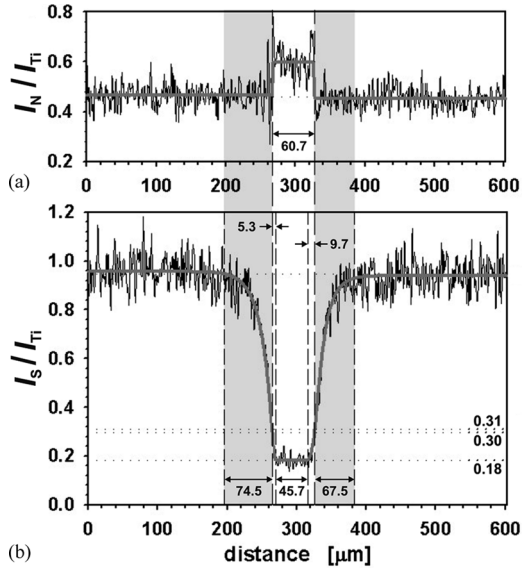

FIGURE 7 Concentration profiles across the epoxy/PVP/epoxy interfaces, as measured by means of EDX. The total length of the profiles is 602 μm. The N- and the S-signals were divided by the signals from the Ti atoms in order to eliminate any variations in the electron beam intensity. (a) From the I_N/I_{Ti}-profile steps are visible which were taken benefit of in order to deduce the edges of the PVP layer. The value of I_S/I_{Ti} at the position of the left- and the right-sided step edges is $\sim$0.30 and 0.31, respectively. Using the characteristic relationship between the I_S/I_{Ti} signal and the concentration ratio r [14], this translates into an r-value of $\sim$0.27. (b) However, the I_S/I_{Ti}- profile exhibits gradients extended over $\sim$71 μm within the epoxy. Very clearly, within the PVP layer the S-concentration is non-zero. Profiles: 2048 data points, dwell time per data point 4 s. The data were slightly smoothed. The grey curves resulted from fit procedures.

The decay zones of the S/Ti-signal are clearly recognisable from Fig. 7b and are shadowed in a grey tone. From the I_S/I_{Ti} profile of Fig. 7b, two major observations can be made:

(i) In the vicinity of PVP (as identified by the high I_N/I_{Ti} signal), the concentration of DDS is significantly reduced (as compared with bulk epoxy) and the total width of the depletion zone is 74.5 and 67.5 μm for the left- and the right-sided epoxy, respectively.
(ii) Within PVP, the concentration of DDS is significantly larger than zero, thus indicating absorption of DDS molecules by the PVP

layer. The concentration of DDS appears to be constant within the central part of the PVP film and shows some rise across the outer regions.

From Monte Carlo simulations of the scattering of electrons of 11.0 keV energy in an epoxy of similar composition, it can be concluded that the lateral resolution of the EDX analysis is in the range of 2–3 μm, which corresponds to the lateral extent of the sub-surface electron scattering plume. This resolution limit is much less than the detected widths of the DDS concentration decays within epoxy and even less than the comparatively narrow decays within the PVP regions. That is, owing to the large extent of these IPs the limit of the spatial resolution of the EDX measurement is negligible.

The DDS concentration gradients can be associated with a chemical IP which is to be compared with the mechanical property variations characterising the mechanical IP. The IP widths of the DDS concentration gradient and the Young's modulus are denoted as w_{DDS} and w_E, respectively. Even though the DDS concentration gradient may not be identical with gradients possibly deduced from other methods sensitive for the chemistry of the system, such as infrared spectroscopy, it reflects local deviations from the stoichiometric balance between amine and epoxy.

For translating the signal intensity profiles from EDX into the corresponding profiles of the amine-epoxy concentration ratio, a reference series of epoxy samples of well defined r-values was analysed. From these data and supporting Monte Carlo simulations a characteristic of the relative intensity $I_{\mathrm{S}}/I_{\mathrm{Ti}}$ was deduced [19]. The profile of the concentration ratio, r, *versus* the distance (as resulting from the application of this characteristic relationship $I_{\mathrm{S}}/I_{\mathrm{Ti}}(r)$ to the signal intensity profile given in Fig. 7b) shows a monotonic decrease from the bulk epoxy value of $r \sim 1$ to a value of ~ 0.27. The latter was taken at the position of the step edges deduced from Fig. 7a. Thus, a strong stoichiometric imbalance is generated within the epoxy IP. It can be attributed to the absorption of DDS by the PVP film.

It should be noted, however, that the above approach of converting the DDS concentration into the amine-epoxy concentration ratio, r, is based on the assumption of negligible concentration variations of DGEBA. Although this approach may not be fully justified and some quantitative deviations from the true r-profile may exist, the pronounced amine depletion is presumed to outweigh the epoxy concentration variations and to entail a drop in the concentration ratio, r. Indeed, in their study involving brominated DGEBA, Oyama *et al*. [12] observed depletion of both amine and epoxy. For the system

corresponding to the present case (initial curing for 2 h at 170°C; PVP-K90), they found total transition widths of 24 and 72 μm, respectively. Thus, there exists a strong difference in the widths of the DDS concentration decays between the present study (on average, $w_{DDS} = 71\,\mu m$, see Fig. 7) and the study by Oyama *et al*. (24 μm). The smaller width observed in their study is consistent with the faster curing rate for their epoxy system containing a 1:1 mixture of standard and brominated DGEBA. According to the references [12,46], at a curing temperature of 175°C the time required for 90% conversion is 57 min for an epoxy mixture with 40% of the brominated DGEBA and 226 min for the neat standard DGEBA. That is, in the case of the standard DGEBA (such as in the present study) a much longer time is available for interdiffusion processes and wider IPs can be expected.

Taking the interphasial decay of the amine concentration (Fig. 7b) together with the modulus-concentration relationship resulting from the DMTA measurements, a profile of the Young's modulus can be deduced. That is, Eq. (2a) can be used to translate the profile of the amine-epoxy concentration ratio, r, into a profile of the Young's modulus, E. A schematic representation of this approach is given in Fig. 8.

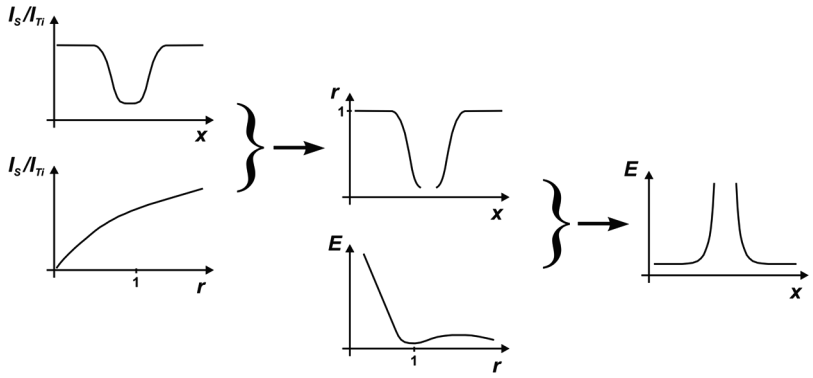

FIGURE 8 Schematic overview of the deduction starting from the amine concentration gradient (resulting from EDX) over the modulus-concentration relationship (resulting from DMTA) to the predicted modulus profile. Combination of the curves indicates an increase in IP modulus with decreasing distance from the interface. Using nanoindentation, this prediction can be tested. The characteristic curve describing the increase in the EDX signal ratio, I_S/I_{Ti}, with the amine-epoxy concentration ratio, r, was derived from measurements of a series of epoxy reference samples in combination with Monte Carlo simulations [14].

Due to the negative slope of the $E'_{heating}(r)$-relationship, the interphasial decrease in the concentration ratio, r, observed when approaching the PVP layer from bulk epoxy, results in an increase in the Young's modulus, E. In order to test this prediction and to provide a characterisation of the mechanical IP, the spatial changes in the Young's modulus as well as in the hardness were mapped by means of nanoindentation.

STUDYING INTERPHASIAL PROPERTY VARIATIONS BY MEANS OF NANOINDENTATION

Analysing Indentation Curves

The indents were arranged along lines with orientation perpendicular to the interfacial borderline between epoxy and the PVP layer. At each indentation point a force-penetration curve, $P(h)$, was recorded, from which mechanical properties can be extracted such as Young's modulus, hardness, or the relative amount of dissipated energy (so-called plasticity index). In short, the Young's modulus, E, is deduced from the slope of the initial part of the unloading curve, the hardness, H, is given by the average contact pressure at maximum load, and the plasticity index, ψ, is calculated from the area enclosed by the loading and the unloading curves. The characteristics of force-penetration curves are depicted in Fig. 9.

According to Oliver and Pharr [30], the loading (l) and the unloading (u) branches can be described as follows:

$$P_l(h) = \alpha\, h^m \tag{4a}$$

$$P_{\mathrm{u}}(h) = \beta(h - h_f)^n, \tag{4b}$$

where h_f denotes the depth of the remaining surface deformation. α and β are constant prefactors. The contact stiffness, S, is given by:

$$S = \frac{dP_{\mathrm{u}}}{dh}\Big|_{P_{\max}} \tag{5}$$

With the values of the Young's modulus, E_t, of the tip material as well as the Poisson's ratio values, ν_s, and ν_t, of sample and tip material, respectively, the Young's modulus of the sample, E_s, can be calculated using the following relationships as given by Hertz's theory [30]:

$$S = 2\, a\, E_{ts} \tag{6}$$

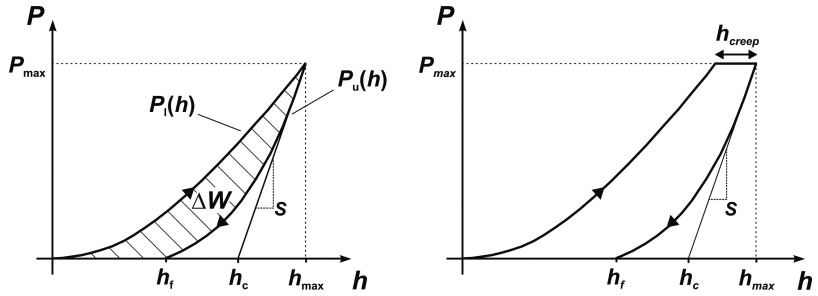

FIGURE 9 Schematic representation of a force-penetration curve $P(h)$ as recorded in the course of a nanoindentation experiment. (a) The two basic periods of the nanoindentation experiment are loading (l) and unloading (u). The Young's modulus is deduced from the initial slope of the unloading branch. (b) Frequently, a hold period is inserted between the loading and the unloading branch, during which creeping can take place.

$$\frac{1}{E_{ts}} = \frac{1-\nu_s^2}{E_s} + \frac{1-\nu_t^2}{E_t}. \tag{7}$$

E_{ts} is the reduced modulus of the tip-sample contact. The contact area, A, can be approximated with a circular area, thus resulting in the contact radius $a = \sqrt{A}/\pi$. For an ideal Berkovich indenter, the dependence of the contact area on the penetration depth is given by $A(h) = c_0 \cdot h^2$ with $c_0 = 24.5$. In general, however, the apex of the tip shows some deviation from the global tip shape, *e.g.* due to blunting. Such imperfections can be described by an extended area function [30,32,47]. Using reference materials, the parameters of the area function are determined by measuring load-displacement curves at various loads [48].

For the evaluation of the epoxy Young's modulus, E_s, the upper portion of the measured unloading curves was described using Eq. (4b), where the constants β, n, and h_f were determined by means of a fitting procedure. The sample modulus, E_s, was calculated using Eqs. (5)–(7). The values of the diamond Young's modulus and Poisson's ratio are $E_t = 1140\,\text{GPa}$ and $\nu_t = 0.069$, respectively. For the epoxy Poisson's ratio, ν_s, the value given in Reference [49] was used, namely, 0.42.

As a measure of the average pressure in the tip-sample contact, the hardness, H, is given by the maximum load, $P_{\max}$, divided by the contact area at the penetration depth, h_c, *i.e.*, at the maximum penetration depth, $h_{\max}$, reduced by the elastic surface deformation

as measured at the periphery of the contact:

$$H = \frac{P_{\max}}{A(h_c)} \tag{8}$$

$$h_c = h_{\max} - k \cdot \frac{P_{\max}}{S}. \tag{9}$$

For Berkovich indenters the value of k is ~ 0.75 [30,47].

A measure of the relative amount of dissipated energy per cycle can be calculated from the area between the loading and the unloading curves, $\Delta W = W_l - W_u$, divided by the total area under the loading curve, W_l [33]:

$$\psi = \frac{\Delta W}{W_l} = \frac{W_l - W_u}{W_l} = \frac{\int P_l(h)dh - \int P_u(h)dh}{\int P_l(h)dh}. \tag{10}$$

In general, this ratio is referred to as plasticity index, ψ. It is indicative of the degree of plastic deformation occurring in the course of the force-penetration experiment. However, strictly speaking, this holds for elastic-plastic materials only ($\psi = 0$ for ideal elastic and $\psi = 1$ for ideal plastic behaviour). In the case of viscoelastic-plastic materials such as glassy polymers, the remaining deformation can contain a slowly relaxing component, depending on the relaxation characteristics of the material and on the hold time of the loading-holding-unloading cycle. Notably, for long hold times the decreasing creep rate is likely to be on the order of the drift rate of the experimental setup. When studying the creep behaviour of a cured epoxy, VanLandingham *et al.* [50] observed such a situation for a hold time of ~ 100 s, corresponding to a creep rate of ~ 0.02 nm/s. In the opposite regime of zero or negligible hold times the presence of a significant creep rate can be observed from the so-called 'nose' effect, *i.e.*, a rounded shape of the force-penetration curve at the maximum load [33,51]. This effect reflects the creep-induced increase in penetration depth when the applied load is kept constant or when the unloading rate is too low.

As shown in Reference [52], ψ can be approximated with the following simple expression:

$$\psi \approx \frac{h_f/h_c}{1 + \frac{C}{E_{ts}/H}}, \tag{11}$$

where $C = \alpha\sqrt{\pi\, c_0}/2$. For a Berkovich indenter, $\alpha \sim 0.75$ and $C \sim 3.29$. For soft matter such as polymers, $E_t >> E_s$ and, approximately, E_{ts} can be replaced with E_s.

It is interesting to note that ψ increases with both the ratios h_f/h_c and E_{ts}/H. The correlation with h_f is obvious from Fig. 9a, since the area of the hysteresis loop increases with h_f. The correlation with E_{ts}/H is consistent with results from elastic-plastic indentation theory by Johnson [53]. According to this, the transition from fully elastic to fully plastic deformation in the tip-sample contact is given by the dimensionless variable $(E/Y) \cdot \tan\beta$. This can be interpreted as the ratio of the strain imposed by the indenter ($\tan\beta$) to the elastic strain capacity of the material (Y/E) [53]. Hereby, Y denotes the yield stress in compression.

The hardness, H, is proportional to the yield strength, Y, as given by Tabor's relationship:

$$H = \kappa \cdot Y. \tag{12}$$

In the case of fully plastic solids deformed in compression, the value of κ is ~ 3. Presumably as a result of a certain amount of elastic strain, however, indentation experiments on poly(ethylene) (PE) delivered values of $\kappa \sim 2$ for yielding in compression and $\kappa \sim 3$ for yielding in tension [54].

Because the ratio E/H provides a measure of the relative amount of plastic deformation, it can be used as a parameter for describing the resistance to scratching and the associated wear phenomena. For instance, Leyland and Matthews [55] emphasised its relevance for assessing the wear resistance of coatings. The tribological performance of coatings requires sufficient hardness as well as some degree of compliance ($1/E$), *i.e.*, low values of the ratio E/H. Due to limited elastic strain and the resulting build-up of high mechanical stresses at the interface with the substrate, however, coatings of both high hardness and high stiffness are more prone to wear than compliant ones.

Mapping Interphasial Variations in Young's Modulus

From the stitched topography image (Fig. 10a), the PVP layer can be readily observed owing to the fact that its surface is higher than the epoxy one. This finding can be attributed to some degree of swelling of the PVP as a result of the uptake of water from the air. PVP is a hygroscopic substance, exhibiting absorption behaviour largely independent of the molecular weight [24]. On the contrary, when measured soon after the microtoming was finished, there was no discernible height step between epoxy and PVP.

The plots of the epoxy Young's modulus values, E_s, *versus* the lateral position of the indentation are given in Figs. 10c and 10d. With decreasing distance, $|x_i\text{-}x|$, from the interface, a significant increase in

E_s occurs. The epoxy bulk modulus value, *i.e.*, the epoxy modulus at a distance far away from the IP, is (3.25 ± 0.07) GPa. The total modulus change from the region more than 300 μm away from the interface to the position at $x = x_i$ is ~ 1.1 GPa.

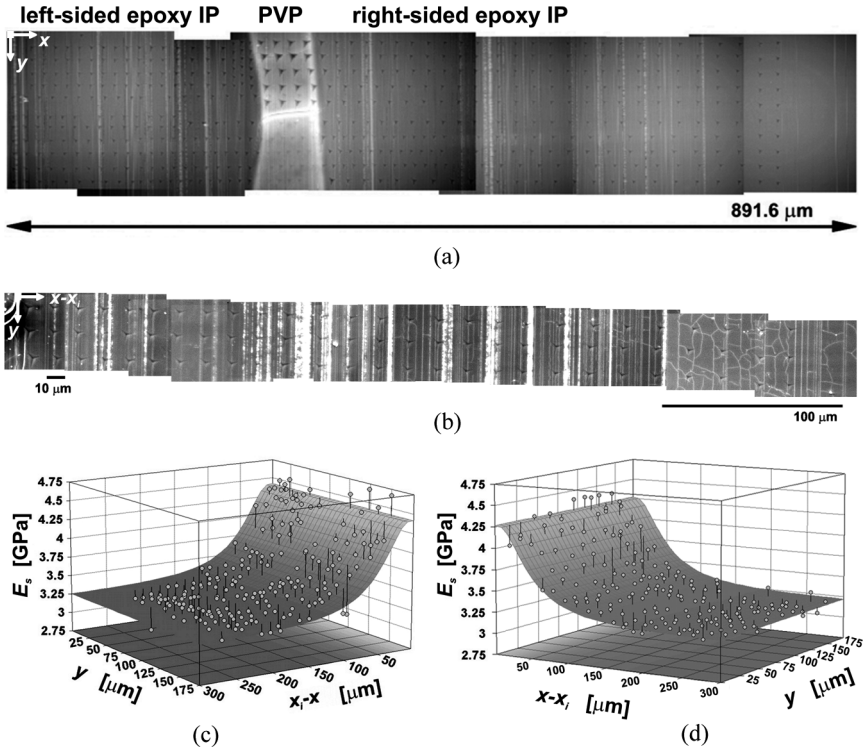

FIGURE 10 (a) Topography image of the field of indentations, recorded after the indentation experiments were finished. The imaging was achieved similar to an AFM in constant force mode, but with the Berkovich indenter as the tip. For covering the large field of indentations, several topography images taken at different positions were stitched together. The scan width was 173 μm. The PVP surface appears bright, because its altitude is higher than that of the epoxy surface. (b) SEM micrographs of the residual imprints of the upper three indentation rows on the right-sided epoxy. The indentation marks adjacent to the interfacial borderline are larger than the residual imprints situated more distant (see also Figure 13). (c) Pseudo-3D-plot of the spatial distribution of the sample Young's modulus values, E_s, measured on the left-sided epoxy IP. The distance from the epoxy-PVP borderline is denoted as x_i-x. (d) Like (c), but for the right-sided epoxy IP. x-x_i denotes the distance from the borderline between PVP and epoxy.

In contrast, for the tangential direction, y, no systematic changes can be stated. Thus, the y coordinate can be neglected and all the data can be projected onto the plane given by E_s and $|x - x_i|$ (Fig. 11a).

A remarkable feature of Fig. 10a is the strong difference in the size of the residual imprints on PVP, since the marks in the upper five indentation rows are much more pronounced than the ones in the lower five rows. This is due to the fact that these measurements were performed 4 weeks later than the first series of indentation rows and some uptake of water from humid air had occurred in the meantime. On epoxy, however, the indentation experiments of the upper five rows did not show any significant differences from the experiments of the lower five rows.

Comparing the Interphasial Profiles of the Various Quantities Deduced From the Force-Distance Curves

The results of the indentation experiments are given in Figs. 11 and 12. In order to enhance the comparability of the different quantities deduced from the indentation experiments, the reduced quantities X/X^b (with $X = E_s$, H, E_s/H, ψ) were plotted, *i.e.*, the ratio with the respective bulk value of the quantity under consideration is given.

As can be seen in Fig. 11b, the hardness, H, exhibits a non-monotonic profile. Its profile is the reverse of that of h_c/h_c^b [52], as consistent with Eq. (8). Using the 1% criterion for defining the demarcation between IP epoxy and bulk epoxy, for H/H^b the resulting width of the epoxy IP is $\sim 230\,\mu m$.

Essentially, the smoothing curve can be divided into four different zones, given by the bulk and three zones within the IP. The various zones can be easily differentiated from each other by their average slopes. In the lower graphs of Fig. 11, the different slopes are indicated using straight lines. The change in these slopes results in kinks which are located at ~ 21 and $\sim 70\,\mu m$, respectively (Table 1). Similar to H, also the profile of the quantity h_c shows four different zones. The total IP width of the h_c/h_c^b profile is $\sim 230\,\mu m$.

An overview of these and the following IP profile characteristics is given in Table 1. Inspection of Table 1 reveals that for the various quantities listed therein, the outer edge of zone Z2 is located at distances between $x_2 \sim 60$ and $\sim 90\,\mu m$. Thus, the x_2 values are comparable with the width of the DDS concentration gradient measured using EDX (Fig. 7).

The ratio E_s/H (Fig. 12a) is dominated by the pronounced changes in E_s (Fig. 11a), *i.e.*, similar to E_s it shows a monotonic increase with decreasing distance $|x - x_i|$. However, the different zones of the

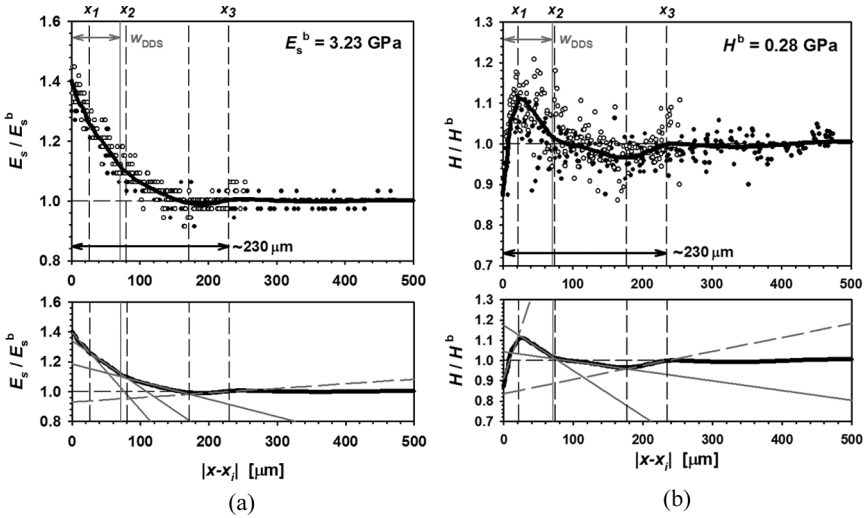

FIGURE 11 Distance dependence of (a) the normalised contact depth, E_s/E_s^b, and of (b) the normalised hardness, H/H^b. Open symbols correspond to the left-sided IP and filled symbols correspond to the right-sided IP, respectively. The curves given in a black solid line resulted from a smoothing procedure. The grey solid line drawn in the vertical direction indicates the average width, w_{DDS}, of the amine depletion zone (EDX). In the lower graphs the slopes of the different IP zones are indicated. Positive and negative slopes are indicated by grey dashed and grey solid lines, respectively.

H-profile induce changes in the slope of the E_s/H-profile. By and large, the profile of E_s/H or $(E_s/H)/(E_s/H)^b$ is similar to that of h_f/h_f^b [52]. With a value of $\sim$230 µm, the IP width resulting from the profile of E_s/H is in agreement with the ones resulting from the H- and the E_s-profiles (within the error margin on the order of $\sim$10 µm).

Notably, the value of $(E_s/H)^b \sim 11.53$ is in reasonable agreement with the typical value of $\sim$10 for the ratio between hardness and the tensile Young's modulus. This value is obtained from Tabor's relationship, Eq. (12), with a value of $\kappa = 3$ for the ratio of hardness and yield strength, and from the relationship $Y \sim E/30$. The latter resulted from studies of molecular materials [54].

From the above results it can be summarised that the profiles of each of the quantities E_s, H, E_s/H, and ψ, indicate an IP where several zones are discernible. In particular, this is true for the hardness, H, where the different zones are most pronounced. Three major IP zones can be distinguished, namely, a thin zone adjacent to the interface (zone Z1), an intermediate zone the right-sided edge of which is

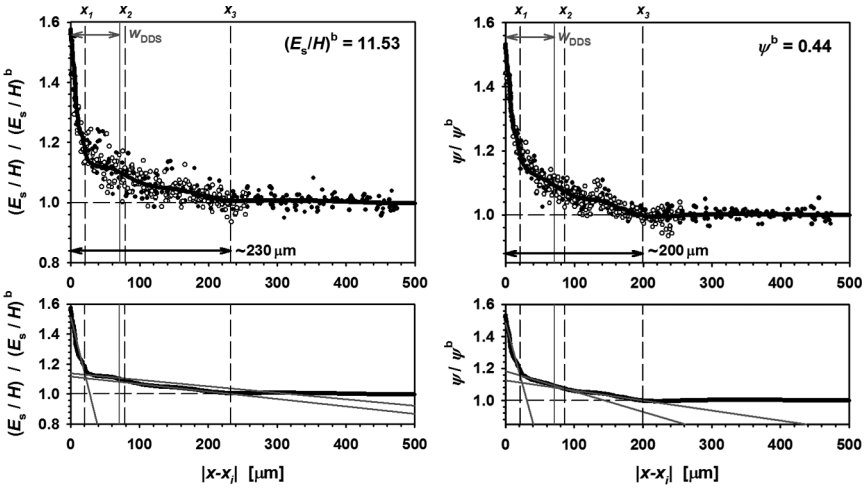

FIGURE 12 Similar to Figure 11, but for (a) $(E_s/H)/(E_s/H)^b$ and (b) ψ/ψ^b, respectively.

located close to the outer edge of the amine depletion zone (zone Z2), and an outer zone ranging up to $\sim$230 μm (see Table 1) away from the PVP/epoxy interface (zone Z3).

Investigation of the Residual Imprints

Further information is available from images of the residual imprints. As shown in the SEM-micrograph given in Fig. 13a, the residual imprints adjacent to the PVP/epoxy interface are significantly larger than the ones farther away from the interface. In terms of the diameter, the imprints in the first column of indentations can be clearly distinguished from the imprints of the second and the following indentation columns (as observed from left to right in Fig. 13a, *i.e.*, with increasing distance from the PVP/epoxy interface). The other residual imprints further away from the interface do not reveal distinct variations in their diameter (Fig. 10b). The ratio of average diameters of the first row of indentations and of all other rows is $\sim$1.3. Hence, a much larger degree of plastic deformation can be stated for the region containing the first column of residual imprints. Since all the indents of this region are located within a distance of less than $\sim$23 μm from the interfacial borderline, the region can be identified with the zone Z1 of the profiles discussed above.

TABLE 1 Overview of the Different IP Zone Edge Positions, x_i $(i = 1, 2, 3)$, as Deduced from the Various Profiles. For Instance, x_1 Denotes the Outer Edge of the Zone Z1. The Zone Widths, w_i, are given by $w_1 = x_1$, $w_2 = x_2 - x_1$, and $w_3 = x_3 - x_2$. The Total IP Width $w_{tot} = w_1 + w_2 + w_3$ is given by x_3

	h_f/h_f^b	h_c/h_c^b	E_s/E_s^b	H/H^b	$(E_s/H)/(E_s/H)^b$	ψ/ψ^b
x_1 [10^2 µm]	0.22	0.21	0.27	0.21	0.21	0.21
x_2 [10^2 µm]	0.6	0.7	0.8	0.7	0.8	0.9
x_3 [10^2 µm]	2.2	2.3	2.3	2.3	2.3	2.0

In the course of an indentation cycle, deformation may occur during the periods of loading and unloading as well as during the hold period. Indeed, the deformation occurring during the latter period, denoted h_{creep}, shows a strong increase within zone Z1, whereas no significant changes can be stated for the zones Z2 and Z3 (Fig. 13b). Considering the quantity h_{creep}/h_{creep}^b, the width of Z1 is $x_1 \sim 24\,\mu m$. This is in reasonable agreement with the values of x_1 as deduced from the other quantities (Table 1).

In summary, zone Z1 is characterised by larger residual imprints, increased creeping, a reduced hardness (Fig. 11b), as well as an increased plasticity index (Fig. 12b). The zone widths can be readily calculated from the zone edge positions given in Table 1. The total width of the IP, w_{tot}, is identical with the outer bound, x_3, of zone Z3. Notwithstanding some variation in the respective zone widths, the width data can be stated to be consistent with each other. When looking at the hardness data, the widths of the three zones Z1–Z3 are $\sim 0.21 \times 10^2$, 0.5×10^2, and $1.6 \times 10^2\,\mu m$, respectively.

Does the Mechanical Bias Effect Need to be Taken Into Account?

It should be noted that interface-related artefacts of the indentation experiments can be ruled out here, owing to the vast extent of the modulus decay. In general, indentations in the close vicinity of an adjacent phase can be affected by its mechanical properties [20,21]. Basically, such a mechanical bias effect is a consequence of the lateral extent of the sub-surface stress distribution. For instance, a corresponding analysis performed at the interface between poly(carbonate) (PC) and steel has shown that the apparent modulus measured on PC is increased at distances, d, lower than the diameter of the final

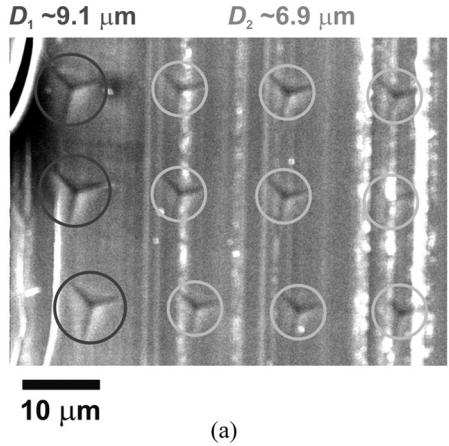

(a)

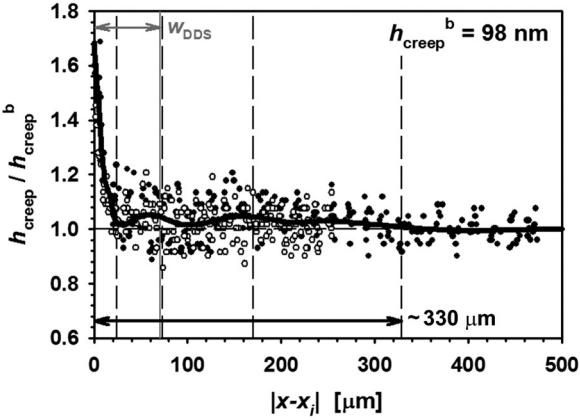

(b)

FIGURE 13 (a) SEM micrograph of indentation marks on the right-sided epoxy, close to the PVP/epoxy interface. The marks belong to the upper three indentation rows. It can be clearly seen that the diameter, D_1, of the marks next to the interface (black circles) is larger than the diameter, D_2, of the marks farther away from the interface (grey circles). On average, the ratio D_1/D_2 is $\sim$1.3. (b) The profile of the viscoelastic creep depth, h_{creep}, occurring during the hold period, shows a pronounced increase within a narrow zone of $\sim$23 μm next to the interface.

residual imprint [29]. Hereby, d denotes the distance between the centre axis of the indenter and the interfacial borderline.

Thus, care was taken to comply with this condition. Furthermore, it is worthwhile noting that the Young's modulus value measured on

PVP is in the range of $E_s \sim 3.9$ GPa and 3.7 GPa, as calculated for PVP Poisson's ratios of $\nu_s \sim 0.35$ and 0.40, respectively. Considering the amorphous nature of PVP, the latter value seems to be more likely. Thus, the PVP modulus is even lower than the epoxy modulus value measured in the close vicinity of the interfacial borderlines. That is, if such a measurement artefact exists it should result in too low a measured epoxy modulus value rather than a too large one. However, E_s was observed to increase in a monotonic manner with decreasing distance $|x - x_i|$ (see below and Reference [19]).

Are the Measurements Likely to be Affected by Strain Gradient Hardening?

Another matter of concern for potential size effects is strain gradient hardening. This effect was reported for various materials as well as for different geometries, see [56] and the references given therein. Although the microscopic hardening mechanisms may depend on the particular class of materials, such as single crystal metals or glassy polymers, it was concluded that as a common characteristic the hardening is associated with the formation of energy absorbing entities, *i.e.*, dislocations, molecular kinks, or activated clusters. As noted by Lam and Chong [56], the general response of various materials to the action of strain gradients suggests that strain gradient hardening is a basic part of micro-scale mechanical behaviour.

The lowest value of the contact depth, h_c, is $\sim 0.94 \cdot h_c^b = 1119$ nm. The total depth of penetration is even larger, typically ranging from ~ 1310 to ~ 1550 nm. According to the investigations by Lam and Chong of an amine-epoxy system [57,58], the upper limit of penetration depths where the measured hardness is affected by strain gradient plasticity is $\sim 1.0\,\mu$m. Due to large strain gradients, for lower indentation depths increased hardness values were observed. For indentations deeper than $\sim 1.0\,\mu$m, however, the strain gradient is negligible and the hardness levels off at a value independent of the contact depth.

Finally, it should be noted that the exclusive consideration of elastic-plastic behaviour implies neglectance of any rate-dependent behaviour potentially affecting the nanoindention results. Owing to the viscoelastic nature of polymer properties, the values of the various quantities considered may slightly depend on the particular rates of loading or unloading. However, the basic finding of various characteristic IP zones should also be valid for higher or lower loading/unloading rates or for different hold times. Moreover, in a recent study by

VanLandingham *et al.* [50], it was shown that in the case of epoxy a large part of creep displacement is due to yield flow. The residual indentation depth was studied as a function of the hold time, in order to explore if the creep response was mainly of a viscoelastic nature or if it included a significant contribution from creep behaviour. Even at low force levels of 50 μN, the viscoelastic creep response was comparatively low.

DISCUSSION OF THE MULTI-ZONE INTERPHASE IN TERMS OF THE INTERFACIAL PROCESSES OCCURRING UPON CURING

A likely reason for the existence of zone Z1 is the bi-directional interdiffusion occurring during the early phase of the curing procedure, where epoxy and amine molecules diffuse into the PVP film and where PVP molecules diffuse into the liquid amine-epoxy mixture. From the existence of zone Z3 additional long-range effects can be inferred. A respective schematic illustration is given in Fig. 14.

Under the presumption of bi-directional interdiffusion, either a blend or an interpenetrating network (IPN) was formed and, in a first approximation, zone Z1 can be described in terms of a mixture of epoxy with PVP. If a mixing rule applies, within zone Z1 the degree of plastic deformation will be in between the respective degrees of bare epoxy and PVP. Indeed, as compared with epoxy the residual imprints on PVP prove a larger degree of plasticity (Fig. 10a). On PVP, the average plasticity index values of the lower and the upper five indentation lines are ~ 0.64 and ~ 0.71, respectively. The increased ψ-value of the upper five indentation lines is a result of the aforementioned uptake of water from humid air. Notably, the ψ-value of ~ 0.64 is very similar to the epoxy ψ-value for $|x - x_i| \to 0$ (Fig. 12b). Thus, it can inferred that the enhanced plasticity observed within zone Z1 is consistent with the statement of a non-zero concentration of PVP within zone Z1 of the epoxy IP.

So far it was assumed that any changes in the relative amine-epoxy concentration ratio, r, are induced by variations in the absolute amine concentration only. In principle, spatial variations can occur for epoxy as well as for amine. By means of an N-layer model, Yang and Pitchumani [11] performed a kinetic analysis of the diffusion and reaction phenomena of a curing epoxy system in the vicinity of an Al fibre. Depending on the adsorption coefficients and the characteristic times for diffusion and reaction, they calculated concentration profiles for amine as well as for epoxy. Although they investigated a different

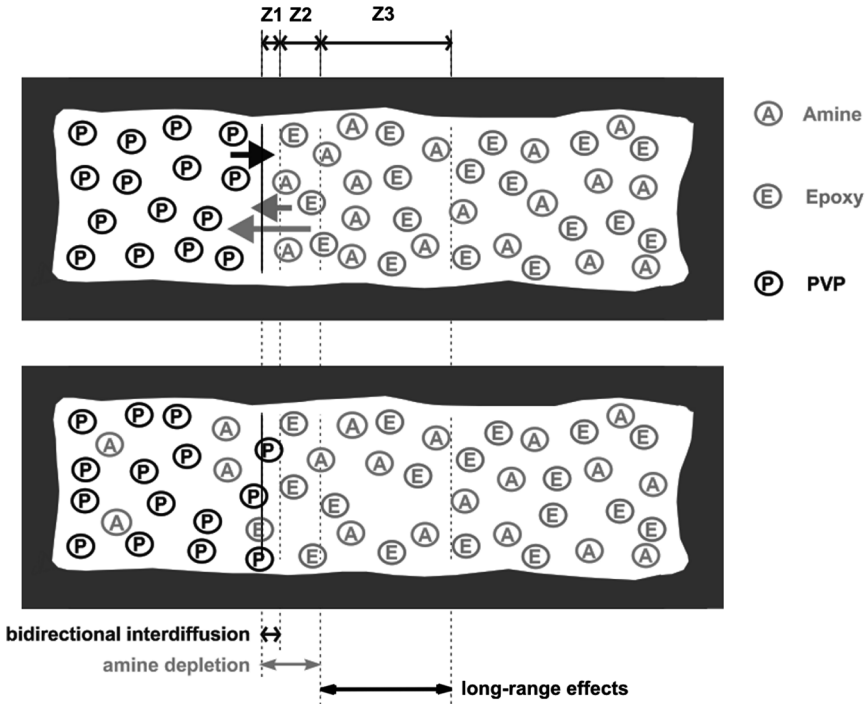

FIGURE 14 Schematic depiction of the three different IP zones identified from the hardness profile. The zone Z1 is likely to be related to a bi-directional interdiffusion (taking place during the curing procedure), whereas the zone Z3 must be attributed to long-range effects acting well beyond the amine depletion zone.

amine-epoxy system, their results show that, similar to the amine and also for the epoxy, extended concentration gradients can be expected. Indeed, in their study of concentration profiles across the PVP/epoxy interface, Oyama *et al.* [12] reported on an epoxy depletion zone about three times wider than the amine depletion zone. However, it should be recalled that they used the aforementioned mixture of the epoxy resin DER332 with a brominated resin, *i.e.*, the curing rate was much higher and, consequently, the time available for interdiffusion was much shorter. This limits the comparatibility with the present study. Firstly, the lower reaction rate of the neat DER332 resin used in this study allows for a larger time window for interdiffusion and, overall, it provokes a wider IP. Yet it is not secure that all species involved benefit to the same degree because the diffusion of bulkier or stiffer

molecules may slow down faster due to the hindrances imposed by the growing network. Secondly, the brominated epoxy molecules used in the study by Oyama *et al.* [12] may affect the driving forces of interdiffusion, *e.g.* by their polarity.

Interestingly, within zone Z3 significant variations in the epoxy mechanical properties are observed, although amine is not found to be deficient within this zone. Long-range effects could be generated due to the diffusional motions induced by the interface. Since the diffusional currents occur simultaneously with the curing reactions, they may interfere with the latter and alter the final network of crosslinks. On the contrary to a quiescent liquid mixture, in the vicinity of the interface the transport of molecular entities leads to anisotropic motions. Such deviations from the isotropic Brownian diffusion can affect the encounters of reaction partners and by this the local reaction rate as well as the final network topology.

For instance, it is worthwhile considering that already existing topologic constraints on the molecular mobility may be mitigated by the interdiffusion processes. The adverse effect of a high crosslink density on the packing efficiency is known from various studies (see [59] and the references therein). Thus, in many cases, close packing may be inhibited due to steric restrictions by the units forming the network. In other words, a high crosslink density can imply a large free volume of the final network. For instance, cage-like topologies are related to a lower overall packing density, since the dense network surrounding a comparatively unoccupied volume (the cage) provides too large a barrier for further amine molecules to enter and add further crosslinks inside. However, by the action of a driving force toward the region of reduced amine concentration, some diffusion barriers become more likely to be surpassed and the probability for accessing the respective free volumes is increased. By such effects related to anisotropic diffusion, much wider an epoxy volume can be affected than the IP volume exhibiting amine depletion. Also in this sense, the mechanical IP can be sub-divided into a DDS depletion zone ($r < 1$) and a solely diffusion-affected zone ($r = 1$).

CONCLUSIONS

In order to study the interphase between the thermoplastic poly(vinylpyrrolidone) (PVP) and an amine-cured epoxy, a stoichiometric amine-epoxy formulation was cured in the presence of a PVP film. The curing was done for 2 h at a temperature of 170°C, *i.e.*, close to the glass transition temperature, T_α, of the PVP.

The nanoindentation data showed that the mechanical property variations are extended over a region of $\sim 230\,\mu m$. One of the most salient observations is that within the interphase, the Young's modulus value is significantly larger than in the bulk epoxy. In particular, it increases when approaching the PVP from the bulk epoxy. These findings are consistent with results from DMTA which show antiplasticization for the excess-epoxy regime ($r < 1$). The antiplasticization effect can be attributed to a suppression of the β-transition around $-70^{\circ}C$, which reflects the coupling between crosslink density and the intensity of local-scale cooperative motions.

Although the Young's modulus profile exhibits pronounced interphasial changes, essentially the profile is monotonic, and from the Young's modulus profile there is no clear indication for the existence of several interphase zones. From the profiles of hardness and plasticity index, however, three different interphase zones can be distinguished. Firstly, the zone next to the PVP layer (zone Z1) is $\sim 21\,\mu m$ wide and shows a strong increase in hardness with increasing distance from the interface. Secondly, the intermediate interphase zone (zone Z2) is extended over $\sim 50\,\mu m$ and is characterised by a pronounced decrease in hardness down to a value similar to the bulk hardness value. Thirdly, the outer interphase zone (zone Z3) features a wide shallow minimum and levels off at the bulk hardness. The position of the minimum of zone Z3 is located at $\sim 180\,\mu m$.

The existence of three different interphase zones was discussed in terms of the interphase formation mechanisms. For zone Z1, the residual imprints were observed to be much larger, and the creep deformation is strongly increased. Considering the large plastic deformation of PVP, this indicates a bi-directional interdiffusion, with amine or epoxy entities moving into PVP and with PVP molecules moving into the epoxy region. The zones Z1 and Z2 lie within the amine depletion region as identified by means of EDX. Finally, the zone Z3 is related to more long-ranging effects, which may be caused by epoxy concentration variations or variations in the crosslink network structure. Considering that the hardness of a material tends to be dominated by structural defects, the hardness variations observed in zone Z3 may indicate imperfections in the network of crosslinks.

Hardness appears to be the most sensitive parameter for interphase property variations. Considering the connection between hardness and yield modulus as given by Tabor's relationship, the material flow is also presumed to show strong spatial variations. Hence, systematic investigations of interfacial failure mechanisms should take into account the variations in the elastic as well as in the plastic properties.

Overall, full coverage of the intricate interphasial property variations requires a set of chemical and mechanical quantities.

ACKNOWLEDGMENTS

The sample preparation, the measurements, as well as major parts of the data evaluation were performed at the Federal Institute for Materials Research and Testing (Bundesanstalt für Materialforschung und –Prüfung, BAM) in Berlin, Germany. A large part of the research was funded by BAM through its Junior Scientist programme. M. M. would like to express his gratitude to H. Sturm and G. Kalinka (both BAM VI.2) for technical assistance with EDX and nanoindentation, respectively. In part, the EDX data were collected by G. Eltanany (formerly BAM VI.2). Her contribution is gratefully acknowledged. Furthermore, the author would like to thank P. Fengler (BAM VI.1) for running the DMTA measurements with great care. M. M. was also involved with a project related to exchange of researchers (PPP) with Spain, funded by the German Academic Exchange Service (DAAD). He appreciates valuable discussions on epoxy characterisation with Prof. I. Mondragon and his working group (Dept. of Chemical Engineering, Univ. of the Basque Country, San Sebastian, Spain). A sample of the epoxy resin DER332 was kindly provided by Nordmann-Rassmann GmbH.

REFERENCES

[1] Jones, R. A. L. and Richards, R. W., *Polymers at Surfaces and Interfaces*, (Cambridge University Press, Cambridge, 1999), Ch. 4.
[2] Sharpe, L. H., *J. Adhesion* **67**, 277–289 (1998).
[3] Schreiber, H. P. and Ouhlal, A., *J. Adhesion* **79**, 141–153 (2003).
[4] Immordino, K. M., McKnight, S. H., and Gillespie, J. W. Jr., *J. Adhesion* **65**, 115–129 (1998).
[5] Gilbert, A. H. and Bucknall, C. B., *Makromol. Chem., Macromol. Symp.* **45**, 289–298 (1991).
[6] Marieta, C., Remiro, P. M., Garmendia, G., Harismendy, I., and Mondragon, I., *European Polym. J.* **39**, 1965–1973 (2003).
[7] Karger-Kocsis, J., Gryshchuk, O., and Schmitt, S., *J. Mater. Sci.* **38**, 413–420 (2003).
[8] Tercjak, A., Serrano, E., Remiro, P. M., and Mondragon, I., *J. Appl. Polym. Sci.* **100**, 2348–2355 (2006).
[9] Gan, W. J., Zhan, G. Z., Wang, M. G., Yu, Y. F., Xu, Y. Z., and Li, S. J., *Colloid Polym. Sci.* **285**, 1727–1731 (2007).
[10] Palmese, G. R. and McCullough, R. L., *J. Adhesion* **44**, 29–49 (1994).
[11] Yang, F. and Pitchumani, R., *J. Appl. Polym. Sci.* **89**, 3220–3236 (2003).
[12] Oyama, H. T., Lesko, J. J., and Wightman, J. P., *J. Polym. Sci. Part B: Polym. Phys.* **35**, 331–346 (1997).

[13] VanLandingham, M. R., Dagastine, R. R., Eduljee, R. F., McCullough, R. L., and Gillespie, J. W. Jr., *Composites Part A* **30**, 75–83 (1999).
[14] González-Benito, J., *J. Colloid Interface Sci.* **267**, 326–332 (2003).
[15] Munz, M., Cappella, B., Sturm, H., Geuss, M., and Schulz, E., *Adv. Polym. Sci.* **164**, 87–210 (2003).
[16] Arvanitopoulos, C. D. and Koenig, J. L., *Appl. Spectrosc.* **50**, 11–18 (1996).
[17] Rajagopalan, G., Immordino, K. M., Gillespie, J. W. Jr., and McKnight, S. H., *Polymer* **41**, 2591–2602 (2000).
[18] Oyama, H. T., Solberg, T. N., and Wightman, J. P., *Polymer* **40**, 3001–3011 (1999).
[19] Munz, M., Sturm, H., and Stark, W., *Polymer* **46**, 9097–9112 (2005).
[20] Li, F., Williams, J. G., Altan, B. S., Miskioglu, I., and Whipple, R. L., *J. Adhesion Sci. Technol.* **16**, 935–949 (2002).
[21] Kumar, R., Cross, W. M., Kjerengtroen, L., and Kellar, J. J., *Compos. Interfaces* **11**, 431–440 (2004).
[22] Hodzic, A., Stachurski, Z. H., and Kim, J. K., *Polymer* **41**, 6895–6905 (2000).
[23] Broyles, N. S., Chen, R., Davis, R. M., Lesko, J. J., and Riffle, J. S., *Polymer* **39**, 2607–2613 (1998).
[24] Bühler, V., *Kollidon–Polyvinylpyrrolidone for the Pharmaceutical Industry*, (BASF - Pharma Ingredients, Ludwigshafen, 2001 6th ed.), Ch. 2.
[25] Tan, Y. Y. and Challa, G., *Polymer* **17**, 739–740 (1976).
[26] Product manual: *DOW Liquid Epoxy Resins*, Midland, DOW Plastics, 1999.
[27] White, S. R., Mather, P. T., and Smith, M. J., *Polym. Engin. Sci.* **42**, 51–67 (2002).
[28] Mathieu, C., Boiteux, G., Seytre, G., Villain, R., and Dublineau, P., *J. Non.-Cryst. Solids* **172–174**, 1012–1016 (1994).
[29] Munz, M., Chung, J., and Kalinka, G., in *Adhesion - Current Research and Applications*, W. Possart (Ed.) (Wiley-VCH, Weinheim, Germany 2005), pp. 103–123.
[30] Oliver, W. C. and Pharr, G. M., *J. Mater. Res.* **7**, 1564–1583 (1992).
[31] Fischer-Cripps, A. C., *Vacuum* **58**, 569–585 (2000).
[32] VanLandingham, M. R., Juliano, T. F., and Hagon, M., *J. Meas. Sci. Technol.* **16**, 2173–2185 (2005).
[33] Briscoe, B. J., Fiori, L., and Pelillo, E., *J. Phys. D: Appl. Phys.* **31**, 2395–2405 (1998).
[34] Verdu, J. and Tcharkhtchi, A., *Angew. Makromol. Chem.* **240**, 31–38 (1996).
[35] Kuchling, H., *Taschenbuch der Physik*, (Verlag Harri Deutsch, Thun, Germany 1985), 5–7th ed., Ch. 12.
[36] Meyer, F., Sanz, G., Eceiza, A., Mondragon, I., and Mijovic, J., *Polymer* **36**, 1407–1414 (1995).
[37] Skourlis, T. P. and McCullough, R. L., *J. Appl. Polym. Sci.* **62**, 481–490 (1996).
[38] Drzal, L. T., Rich, M. J., Koenig, M. F., and Lloyd, P. F., *J. Adhesion* **16**, 133–152 (1983).
[39] Nielsen, L. E., *J. Macromol. Sci. –Rev. Macromol. Chem. C* **3**, 69–103 (1969).
[40] Calventus, Y., Montserrat, S., and Hutchinson, J. M., *Polymer* **42**, 7081–7093 (2001).
[41] Yim, H., Kent, M., McNamara, W. F., Ivkov, R., Satija, S., and Majewski, J., *Macromolecules* **32**, 7932–7938 (1999).
[42] Lee, H. and Neville, K., in *Handbook of Epoxy Resins*, (McGraw-Hill, New York, 1967), Ch. 8.
[43] Heux, L., Halary, J. L., Lauprêtre, F., and Monnerie, L., *Polymer* **38**, 1767–1778 (1997).
[44] Heux, L., Lauprêtre, F., Halary, J. L., and Monnerie, L., *Polymer* **39**, 1269–1278 (1998).

[45] Soles, C. L. and Yee, A. F., *J. Polym. Sci. Part B: Polym. Phys.* **38**, 792–802 (2000).
[46] Naé, H. N., *J. Appl. Polym. Sci.* **33**, 1173–1185 (1987).
[47] Bao, Y. W., Wang, W., and Zhou, Y. C., *Acta Materialia* **52**, 5397–5404 (2004).
[48] Herrmann, K., Jennett, N. M., Wegener, W., Meneve, J., Hasche, K., and Seemann, R., *Thin Solid Films* **377–378**, 394–400 (2000).
[49] Verdu, J. and Tcharkhtchi, A., *Angew. Makromol. Chem.* **240**, 31–38 (1996).
[50] VanLandingham, M. R., Chang, N.-K., Drzal, P. L., White, C. C., and Chang, S.-H., *J. Polym. Sci.: Part B: Polym. Phys.* **43**, 1794–1811 (2005).
[51] Tweedie, C. A. and Van Vliet, K. J., *J. Mater. Res.* **21**, 1576–1589 (2006).
[52] Munz, M., *J. Phys. D: Appl. Phys.* **39**, 4044–4058 (2006).
[53] Johnson, K. L., *Contact Mechanics*, (Cambridge University Press, Cambridge, 1985), Ch. 6.
[54] Baltá Calleja, F. J. and Fakirov, S., *Microhardness of Polymers*, (Cambridge Solid State Science Series, Cambridge University Press, Cambridge, 2000), Ch. 4.
[55] Leyland, A. and Matthews, A., *Wear* **246**, 1–11 (2000).
[56] Lam, D. C. C. and Chong, A. C. M., *Mater. Sci. Eng. Part A* **318**, 313–319 (2001).
[57] Chong, A. C. M. and Lam, D. C. C., *J. Mater. Res.* **14**, 4103–4110 (1999).
[58] Lam, D. C. C. and Chong, A. C. M., *Mater. Sci. Eng. Part A* **281**, 156–161 (2000).
[59] Morgan, R. J., *Adv. Polym. Sci.* **72**, 1–43 (1985).